Embedded-cluster self-consistent partial-wave method: Extending the spatial scale of electronic structure calculations

Frank W. Averill[1,2] and Gayle S. Painter[1,*]
[1]*Materials Science and Technology Division, Oak Ridge National Laboratory, Oak Ridge, Tennessee 37831-6114, USA*
[2]*Center for Materials Processing, University of Tennessee, Knoxville, Tennessee 37996-0750, USA*
(Received 19 November 2007; published 8 April 2008)

An efficient approach to extending the spatial scale of electronic structure calculations is described in this work. The method is formulated as a combination of the "interacting fragments" concept of Harris [Phys. Rev. B **31**, 1770 (1985)] and the divide and conquer (D&C) method of Yang [Phys. Rev. Lett. **66**, 1438 (1991); Phys. Rev. A **44**, 7823 (1991)], which recognizes the intrinsic locality of electron bonding and is devised to optimize the total electron charge density within an approximate representation of partitioned components. Beginning with a brief review of D&C concepts, we report results from this method using the D&C as an "embedding" method for coupling an atomic cluster to its extended environment. The convergence properties as implemented within the self-consistent partial-wave (SCPW) linear variational method are illustrated through various applications. In particular, results from a study of the adsorption of La atoms at the prism plane of β-Si_3N_4 demonstrate the practicality of the SCPW using D&C as an embedding technique.

DOI: 10.1103/PhysRevB.77.155109 PACS number(s): 71.15.−m, 61.46.Bc, 31.15.E−, 31.50.Bc

I. INTRODUCTION

In his original paper,[1] Yang introduced the divide and conquer (D&C) method as a way of overcoming the order N^3 problem that makes the *ab initio* and first-principles solution of the wave equation for large molecules increasingly costly as the number of atoms, N, increases. Essentially, Yang's method "partitions" a large molecule into Ω smaller molecular fragments (with fragment i having $\sim N_i$ atoms where $N_i \ll N$). In the local density approximation (LDA) the one-electron equation of each partition is then solved self-consistently in the potential field of all the fragments. In this way, the order N^3 problem of the larger molecule is reduced to a sum over Ω order $-N_i^3$ problems, where $\Sigma_i^{\Omega} N_i^3 \ll N^3$. The accuracy of the D&C method is only limited by how well the electronic density within each partition or fragment reproduces the true self-consistent density of the larger molecule in that partition.

At the lowest level approximation, which we label D&C(0), the one-electron equation for each fragment is solved [e.g., within the linear combination of atomic orbitals (LCAO) method] using only basis functions corresponding to the atoms in that fragment. In general, D&C(0) would not be very accurate since in such an approximation atoms in a given partition would interact with atoms in another only through their classical Coulomb fields. (Of course, when the two partitions in question are widely separated the atoms in separate partitions would indeed interact only classically.) The D&C(0) approximation may be improved upon by supplementing the basis set in each partition with basis functions associated with atoms (called buffer atoms[1]) outside of, but adjacent to, the given partition. After calculating the electronic density of each "buffered" atom cluster, the densities of the buffer atoms lying outside the original fragments are effectively truncated by multiplying the density of each α fragment by a partition function, P^{α}. In principle, a precise result within the LCAO approximation is obtained if each fragment is buffered with all the atoms outside the fragment. However, this would defeat the purpose of the method in that as much work would go into solving the wave equation for each fragment as would be expended in solving that for the original large molecule directly. The usefulness of D&C depends upon obtaining sufficient accuracy for a specific problem with a modest amount of buffering. This approach is supported by the now widely recognized concept of the "nearsightedness" of electrons[2] which suggests that the spatial range of quantum interactions of electrons is usually limited. Numerous successful applications of D&C[3–17] in the literature, as well as the success of subsequent order-N methodologies,[18] give further credence to the D&C concept.

In a recent paper,[19] the authors used the self-consistent partial-wave (SCPW) method[20] in a study of the convergence of ground state properties and equilibrium structures of molecules as approximate representations of the electron charge density were systematically improved. By its construct, the SCPW method treats atomic clusters with precision that can be controlled within specified regions. Thus an "active region" of a cluster can be treated with high precision, whereas certain approximations can be evoked for the remainder. In this sequel work, we investigate the potential of D&C as an embedding scheme within the SCPW framework. Our approach is in the spirit of the embedded-cluster method of Zhu, *et al.*,[7] however, it differs in some details. Within D&C embedding, a finite atom cluster is used to simulate the local effect of an impurity or defect within a solid or at a solid surface. In order to reduce the computational effort, the impurity and its first few shells of neighboring atoms are chosen as one of the D&C partitions and the remaining atoms, representing the so called "external" environment, are partitioned into one or more additional fragments. Besides the reduction in the N^3 computational effort afforded by D&C, this approach also provides a simple way of computationally separating the two physical regions (impurity region and external environment).[21] It is commonly assumed[22] that a minimal number of approximations and an extensive basis set should be used in the impurity region, while less precise

models can be used elsewhere. The D&C method provides the means for a smooth transition from one spatial region and level of approximation to another.

Many of the constructs used in the original D&C method (e.g., density partitioning, numerical integration, and atom-centered partial-wave expansions for densities and potentials) are already components of the SCPW method, such that D&C is straightforward to implement in a controlled way. Sections II A and II B give some of the details of this implementation, including a discussion in Sec. II C of the computation of the kinetic and potential energies within D&C. In Sec. II D the problem of computing forces on atoms in the D&C approximation is considered by deriving an analytical expression for the force as the derivative of the D&C energy. Zhao and Yang[5] heuristically obtained a different expression for the D&C force by applying D&C concepts to the rigorous analytical expression for the gradient force associated with the Harris energy. They showed that their expression converges to the gradient of the D&C energy, but only if they buffered each D&C fragment with many shells of neighboring atoms. In Sec. II D, an expression for the D&C force is given which accurately gives the gradient of the D&C energy independent of the level of buffering.

Section III begins with a brief review of computational details (Sec. III A) followed by three applications of D&C, including the N_2 molecule (Sec. III B) where it is shown that the new expression for the gradient force accurately tracks the numerical derivative of the D&C energy. For purposes of illustrating the effect of buffering on the equilibrium geometry of a molecule, a trivial application of D&C to the formamide molecule ($HCONH_2$) is given in Sec. III C. Divide and conquer as an embedding technique is covered in Sec. III D where we examine a model of the adsorption of La atoms on the prism plane surface of β-Si_3N_4 grains as an illustration. Section IV provides a summary with conclusions.

II. COMBINED DIVIDE AND CONQUER SELF-CONSISTENT PARTIAL-WAVE METHOD

A. Relationship between divide and conquer and the Harris total energy expression

Yang's elegant development[1] of D&C was based upon approximating the Kohn–Sham (KS) energy; here we present a different approach that views D&C as an approximation to the total energy expression in Harris's treatment[23,24] of interacting fragments. Although the final result will be the same as Yang's, some insights are gained along the way. It should be pointed out that in his initial introduction of D&C,[1] Yang used a real space function to partition the electronic density, and we adopt that here. Later, Yang and Lee[6] introduced a form of partitioning using the density matrix that is now widely implemented in various modified forms. In the present work, only the original real space form of D&C will be discussed.

Within the formulation of Harris, the total energy of an assembly of atoms is written in the Born–Oppenheimer approximation[25] as[23,24,26]

$$E_H = \sum_i^M n_i \varepsilon_i - \int \rho_I(\vec{r}) \left[\frac{1}{2} \phi_I(\vec{r}) + \mu_{xc}^I(\vec{r}) \right] d\vec{r} + E_{xc}[\rho_I] + E_{NN}, \tag{1}$$

where the sum is over M occupied one-electron states with energies $\{\varepsilon_i\}$ and occupation numbers $\{n_i\}$ that are solutions of the associated one-electron equation,

$$\left[-\frac{1}{2}\nabla^2 + \phi_I(\vec{r}) + V_N(\vec{r}) + \mu_{xc}^I(\vec{r}) \right] \psi_i(\vec{r}) = \varepsilon_i \psi_i(\vec{r}). \tag{2}$$

Here ρ_I is the "input" electronic density used to construct the associated Coulomb potential, ϕ_I, the exchange-correlation potential, μ_{xc}^I, and the total exchange-correlation energy, E_{xc}. The contributions of the atomic nuclei to the Coulomb potential and total energies are, respectively, V_N and E_{NN}. In the original Harris procedure,[23] Eq. (2) is not iterated to self-consistency and the total energy in Eq. (1) is solely dependent upon the basis set and the choice of input density, ρ_I. The advantage of Eq. (1) over the standard Kohn–Sham energy, which explicitly includes the electronic kinetic energy but not the one-electron energies $\{\varepsilon_i\}$, is that first-order errors in the input density, ρ_I, produce only second-order errors in the total energy, E_H.

Yang[1] introduced the concept of D&C with an expression similar to Eq. (1), which is derived from the KS total energy,[27] where at self-consistency the input density, ρ_I, is assumed to equal the output density ρ_O generated by the sum over all one-electron states,

$$\rho_O(\vec{r}) = \sum_i^M n_i |\psi_i(\vec{r})|^2. \tag{3}$$

The D&C is thus a self-consistent method generating the input density; in contrast, Harris's input density is an approximation to the output density. Yang later introduced approximations for the input density by defining a partitioning operator,P^α, for each molecular fragment defined such that the total density is represented by a sum over Ω molecular fragment densities ρ_I^α determined by the M^α states of each fragment as follows:

$$\rho_I(\vec{r}) = \sum_\alpha^\Omega \rho_I^\alpha = \sum_\alpha^\Omega P^\alpha(\vec{r}) \sum_i^{M^\alpha} n_i^\alpha |\psi_i^\alpha(\vec{r})|^2. \tag{4}$$

The specifics of the partition function P^α are somewhat arbitrary, but it must have the property of being close to unity near atoms in fragment α, while falling off rapidly to zero near atoms outside the fragment. Its purpose is to smoothly join the densities of adjacent fragments, while limiting the overlap of their densities. Yang introduced a fragment partition function in terms of the spherically averaged free atom densities, $\{\rho_i^2\}$ of the atoms composing the fragment. For a given fragment α,

$$P^\alpha(\vec{r}) = \frac{g^\alpha(\vec{r})}{\sum_\beta^\Omega g^\beta(\vec{r})}, \tag{5}$$

where

$$g^{\beta}(\vec{r}) = \sum_{k}^{\text{atoms in } \beta} [\rho_k(r_k)]^2, \tag{6}$$

and $r_k \equiv |\vec{r} - \vec{R}_k|$. The k sum runs over atoms in positions $\{\vec{R}_k\}$ within the given fragment, β. The sum over eigenvalues of the M-state system can be obtained in approximate form from those of the Ω fragments, with partition α having M^{α} states. This is done by weighting the eigenvalue sum of fragment α according to the occupancy and partitioned charge integral of each state in the fragment,

$$\sum_{i}^{M} n_i \varepsilon_i \approx \sum_{\alpha}^{\Omega} \sum_{i}^{M^{\alpha}} n_i^{\alpha} \varepsilon_i^{\alpha} \left(\int P^{\alpha}(\vec{r}) |\psi_i^{\alpha}(\vec{r})|^2 d\vec{r} \right). \tag{7}$$

This expression reflects the major advantage of the D&C approach, i.e., replacing the eigenvalue problem for the M-state system by a number (Ω) of smaller M^{α} state systems ($M_{\alpha} \ll M$). The M^{α} one-electron eigenfunctions $\{\psi_i^{\alpha}\}$ of the α molecular fragment are solutions to the one-electron equation

$$\left[-\frac{1}{2}\nabla^2 + \phi_I(\vec{r}) + V_N(\vec{r}) + \mu_{xc}^I(\vec{r}) \right] \psi_i^{\alpha}(\vec{r}) = \varepsilon_i^{\alpha} \psi_i^{\alpha}(\vec{r}). \tag{8}$$

Solutions in partition α are expanded in basis functions primarily associated with atoms belonging to the α molecular fragment. However, the orbitals on "buffer atoms" can also be chosen to supplement a given fragment's LCAO expansion, although they are defined on atoms that lie outside the partition. The one-electron potentials ϕ_I and μ_{xc}^I in Eq. (8) are calculated from the D&C total density ρ_I defined in Eq. (4) and the nuclear potential V_N includes all sites in the total system. Self-consistent solutions to Eq. (8) are found iteratively and simultaneously for all Ω fragments of the original molecule. Following usual procedures, at the end of each iteration, a new input density ρ_I is obtained from Eq. (4) and the one-electron potentials from this density are determined for the next iteration of Eq. (8) for each fragment α.

The occupation numbers for a fragment $\{n_i^{\alpha}\}$ can in principle be determined by usual zero-temperature Fermi statistics such that $n_i^{\alpha}=1$ for those levels with one-electron energies $\{\varepsilon_i^{\alpha}\}$ below the Fermi energy ε_F and $n_i^{\alpha}=0$ for levels above it. However, with the density partitioning described in Eq. (4), occupied valence states no longer necessarily contribute a full electron to the total charge. In D&C such states contribute a reduced charge, η_i^{α}, given by

$$\eta_i^{\alpha} = n_i^{\alpha} \int P^{\alpha}(\vec{r}) |\psi_i^{\alpha}(\vec{r})|^2 d\vec{r} \tag{9}$$

to the total input charge of the system, where $\eta_i^{\alpha} \leqslant n_i^{\alpha}$. That is, the fragment occupation numbers $\{n_i^{\alpha}\}$ are essentially scaled by the partition operator to the amount of charge inside the given fragment. Therefore the one-electron levels must be filled in order of increasing energy until the total number of the electrons N_e in the system is reached in which case the $\{\eta_i^{\alpha}\}$ satisfy

$$\sum_{\alpha}^{\Omega} \sum_{i}^{M^{\alpha}} \eta_i^{\alpha} = N_e. \tag{10}$$

In zero-temperature Fermi statistics, the Fermi energy ε_F is the same as (or slightly above) that of the last occupied level. However, as a result of partitioning [see Eq. (9) and the condition of Eq. (10)], the occupation number n_i^{α} of a level near ε_F can range between 0 and 1. In iterative calculations, where two or more levels fall at the Fermi energy, the levels can be partially occupied at ε_F, such that a local minimum in the total energy is obtained. Achieving stability of the system as occupation numbers change can be rather challenging in some cases. A rather elaborate method[28] based upon "steepest descent" treats the comparable problem in traditional KS calculations. However, in this work we follow the simpler approach used by Yang for dealing with cases of competing levels at or near the Fermi energy in his development of D&C. In this method,[1] based upon finite temperature Fermi statistics, an inverse temperature B is chosen and occupation numbers are evaluated using the Fermi function, f_B, according to the separation of the corresponding eigenvalues from ε_F as follows:

$$n_i^{\alpha} = f_B(\varepsilon_F - \varepsilon_i^{\alpha}) = \frac{1}{1 + e^{-B(\varepsilon_F - \varepsilon_i^{\alpha})}}. \tag{11}$$

For a selected B the Fermi energy must yield $\{\eta_i^{\alpha}\}$ satisfying Eq. (10). For a given temperature and Fermi energy, the contribution of each eigenfunction to the total charge [i.e., Eq. (9)] can be evaluated by a simple matrix multiplication involving the raw basis functions (or symmetry orbitals) $\{\phi_k^{\alpha}\}$ and eigenvectors $\{c_{ik}^{\alpha}\}$ of a given iteration as

$$\eta_i^{\alpha} = n_i^{\alpha} \sum_{j}^{M^{\alpha}} \sum_{k}^{M^{\alpha}} c_{ij}^{*\alpha} c_{ik}^{\alpha} s_{jk}^{\alpha}, \tag{12}$$

where

$$s_{jk}^{\alpha} = \int P^{\alpha}(\vec{r}) \phi_j^{*\alpha}(\vec{r}) \phi_k^{\alpha}(\vec{r}) d\vec{r}. \tag{13}$$

These "partitioned-overlap integrals" $\{s_{jk}^{\alpha}\}$ can be evaluated initially and then used through all iterative cycles to find η_i^{α} for a given ε_F. In each cycle, the Fermi energy is determined by variation to enforce charge conservation [Eq. (10)]. The evaluation of the Fermi energy, even at finite temperature, is therefore straightforward. Selection of the inverse temperature B is arbitrary; however, it suffices to choose a large enough B that still ensures that the occupation numbers in Eq. (11) and the η_i^{α} that depend upon them vary smoothly with the Fermi energy. This inverse temperature is retained throughout any series of related calculations.

In summary, the D&C total energy can be written as

$$E_{D\&C} = \sum_{\alpha}^{\Omega} \sum_{i}^{M^{\alpha}} \eta_i^{\alpha} \varepsilon_i^{\alpha} - \int \rho_I(\vec{r}) \left[\frac{1}{2} \phi_I(\vec{r}) + \mu_{xc}(\vec{r}) \right] d\vec{r} + E_{xc}[\rho_I] + E_{NN}, \tag{14}$$

where the one-electron energies, $\{\varepsilon_i^{\alpha}\}$, correspond to the self-

consistent solutions of Eq. (8), the input density ρ_I is obtained from Eq. (4), and the partitioned-occupation numbers, $\{\eta_i^\alpha\}$, are given by Eq. (12).

B. Solving Poisson's equation in the self-consistent-partial-wave method

For each iteration in the self-consistent solution of Eq. (8), the Coulomb potential due to the input charge density ρ_I [Eq. (4)] must be evaluated. In the SCPW[19,20] method, this is accomplished by first subtracting from ρ_I the sum of the spherically averaged densities ρ_k of the constituent atoms to yield a difference density

$$d(\vec{r}) = \rho_I(\vec{r}) - \sum_k^{\text{all atoms}} \rho_k(r_k). \tag{15}$$

The advantage of this subtraction process is that it largely removes the rapidly changing core density from the total density, and thereby allows use of fewer points in the radial partial-wave grids. The remaining difference density [Eq. (15)] is in turn written as a sum of atom-centered partial waves[29,30] using a projection technique described in detail in Refs. 20 and 29. The result is that the input density ρ_I [Eq. (4)] can be approximated with controlled accuracy by the quantity

$$\tilde{\rho}_I(\vec{r}) = \sum_k^{\text{all atoms}} \left[\rho_k(r_k) + \sum_{l=0}^{l_{\max(k)}} \sum_{m=-l}^{l} \rho_{lm}^k(r_k) y_{lm}^k(\hat{r}_k) \right], \tag{16}$$

where $l_{\max(k)}$ is the largest l value of the partial-wave expansion on atom site k. This approximate density is, along with all dependent potentials and energies, denoted with a tilde in subsequent expressions. In principle, this approximation for ρ_I can be made arbitrarily accurate by increasing $l_{\max(k)}$. In Ref. 19, the authors showed that within the SCPW, $l_{\max(k)}=2$ gives bond distances in a particular set of molecules to within ± 0.01 Å.

The Coulomb potentials v_k and v_{lm}^k are directly calculated from the atom density ρ_k and the partial-wave density ρ_{lm}^k, respectively. The potential of $\tilde{\rho}_I$ can then be exactly expressed as

$$\tilde{\phi}_I(\vec{r}) = \sum_k^{\text{all atoms}} \left[v_k(r_k) + \sum_{l=0}^{l_{\max(k)}} \sum_{m=-l}^{l} v_{lm}^k(r_k) y_{lm}(\hat{r}_k) \right]. \tag{17}$$

Introducing $\tilde{\rho}_I$ as an approximation to ρ_I, the D&C total energy [Eq. (14)] and the one-electron equation [Eq. (8)] are given by

$$\tilde{E}_{D\&C} = \sum_\alpha^\Omega \sum_i^{M^\alpha} \eta_i^\alpha \varepsilon_i^\alpha - \int \tilde{\rho}_I(\vec{r}) \left[\frac{1}{2}\tilde{\phi}_I(\vec{r}) + \tilde{\mu}_{xc}(\vec{r}) \right] d\vec{r} + E_{xc}[\tilde{\rho}_I] + E_{NN} \tag{18}$$

and

$$\left[-\frac{1}{2}\nabla^2 + \tilde{\phi}_I(\vec{r}) + V_N(\vec{r}) + \tilde{\mu}_{xc}^I(\vec{r}) \right] \psi_i^\alpha(\vec{r}) = \varepsilon_i^\alpha \psi_i^\alpha(\vec{r}). \tag{19}$$

The only difference between the potential sets $\{\tilde{\phi}_I, \tilde{\mu}_{xc}^I\}$ and $\{\phi_I, \mu_{xc}^I\}$ is that the first set is evaluated from $\tilde{\rho}_I$ and the second from ρ_I.

C. Kinetic and potential energies

It is possible to obtain compatible D&C expressions for kinetic and potential energies by solving Eq. (19) for the one-electron energy ε_i^α and substituting that expression into Eq. (18), giving a new but equivalent expression for $\tilde{E}_{D\&C}$ as follows:

$$\tilde{E}_{D\&C} = \sum_\alpha^\Omega \sum_i^{M^\alpha} \eta_i^\alpha k_i^\alpha + \int \tilde{\rho}_o(\vec{r}) [\tilde{\phi}_I(\vec{r}) + V_N(\vec{r}) + \tilde{\mu}_{xc}(\vec{r})] d\vec{r} - \int \tilde{\rho}_I(\vec{r}) \left[\frac{1}{2}\tilde{\phi}_I(\vec{r}) + \tilde{\mu}_{xc}(\vec{r}) \right] d\vec{r} + E_{xc}[\tilde{\rho}_I] + E_{NN}, \tag{20}$$

where

$$k_i^\alpha = \int \psi_i^{\alpha *} \left[-\frac{1}{2}\nabla^2 \right] \psi_i^\alpha(\vec{r}) \tag{21}$$

and

$$\tilde{\rho}_o(\vec{r}) = \sum_\alpha^\Omega \sum_i^{M^\alpha} \eta_i^\alpha |\psi_i^\alpha(\vec{r})|^2. \tag{22}$$

The above sum of fragment densities, $\tilde{\rho}_o$, will also be referred to as an "output" density in that it is formed from the solutions of Eq. (19). It is interesting to compare this new output density, $\tilde{\rho}_o$, with the input density $\tilde{\rho}_I$ given in Eq. (16). They are both approximations to the KS density ρ_o in Eq. (3), but differ in how D&C partitioning is accomplished. For $\tilde{\rho}_o$ [Eq. (22)], partitioning comes from the partitioned-occupation numbers $\{\eta_i^\alpha\}$ as defined in Eqs. (10)–(13). Partitioning enters $\tilde{\rho}_I$ through Eq. (16) and ρ_I in Eq. (4).

Equation (20) can be transformed into a simpler expression by adding and subtracting the term $1/2\int \tilde{\rho}_I(\vec{r})[\tilde{\phi}_I(\vec{r})]d\vec{r}$ and introducing the difference density

$$\Delta\tilde{\rho}(\vec{r}) = \tilde{\rho}_o(\vec{r}) - \tilde{\rho}_I(\vec{r}), \tag{23}$$

giving

$$\tilde{E}_{D\&C} = \sum_\alpha^\Omega \sum_i^{M^\alpha} \eta_i^\alpha k_i^\alpha + \int \tilde{\rho}_I(\vec{r}) \left[V_N(\vec{r}) + \tfrac{1}{2}\tilde{\phi}_I(\vec{r}) \right] d\vec{r} + E_{xc}[\tilde{\rho}_I] + E_{NN} + \int \Delta\tilde{\rho}(\vec{r}) [V_N(\vec{r}) + \tilde{\phi}_I(\vec{r}) + \tilde{\mu}_{xc}(\vec{r})] d\vec{r}. \tag{24}$$

The first term in Eq. (24),

$$K0_{D\&C} = \sum_{\alpha}^{\Omega} \sum_{i}^{M^{\alpha}} \eta_i^{\alpha} k_i^{\alpha}, \tag{25}$$

is the D&C approximation to the KS kinetic energy of the noninteracting electron gas of density ρ_o given in Eq. (3). Furthermore, both Eqs. (20) and (24) can be viewed as approximations[26] for the Kohn–Sham energy of the electronic density ρ_o, accurate to first order in $\Delta\tilde{\rho}$ (although ρ_o is approximated by $\tilde{\rho}_o$ in computing $\Delta\tilde{\rho}$). Similarly, the last term of Eq. (24) yields the first-order corrections to the electron-nuclear, electron-electron, and exchange-correlation energies.

From Eq. (24), it is easily shown that $\tilde{E}_{D\&C}$ becomes stationary (i.e., $\delta\tilde{E}_{D\&C}=0$) when ψ_i^{α} satisfies the one-electron equation, Eq. (19). This relationship between Eqs. (18) and (19) ensures that first-order errors in ψ_i^{α} will produce at most second-order errors in $\tilde{E}_{D\&C}$.

Equation (25) can be used to derive a D&C expression for the kinetic energy of the *interacting* electron system. It has been shown that within the LDA, the exchange-correlation contribution to the kinetic energy density can be expressed in terms of the exchange-correlation potential μ_{xc} and energy density ε_{xc} as[31,32]

$$t_{xc}(\vec{r}) = 3\mu_{xc}(\vec{r}) - 4\varepsilon_{xc}(\vec{r}). \tag{26}$$

This relationship and Eq. (18) suggest that appropriate expressions for the D&C kinetic and potential energies in the LDA are, respectively,

$$\widetilde{KE}_{D\&C} = \sum_{\alpha}^{\Omega} \sum_{i}^{M^{\alpha}} \eta_i^{\alpha} k_i^{\alpha} + 3\int \tilde{\rho}_I(\vec{r})[\tilde{\mu}_{xc}^{I}(\vec{r})]d\vec{r} - 4\tilde{E}_{xc}[\tilde{\rho}_I] \tag{27}$$

and

$$\widetilde{PE}_{D\&C} = \tilde{E}_{D\&C} - \widetilde{KE}_{D\&C}. \tag{28}$$

Comparable expressions can in principle be obtained in the generalized gradient approximation[33] (GGA); however, the GGA exchange-correlation contribution to the kinetic energy density involves additional terms[34] beyond those given in Eq. (26).

D. Evaluation of the divide and conquer gradient force

The x coordinate of the force on the pth nucleus can be formally obtained by computing the derivative of the total energy $\tilde{E}_{D\&C}$ with respect to the pth nuclear coordinate, $\partial\tilde{E}_{D\&C}/\partial X_p$. In computing the derivative of one-electron energies, it will be useful to make use of the following equivalent expressions:

$$\varepsilon_i^{\alpha} = \int \psi_i^{*\alpha}(\vec{r}) H \psi_i^{\alpha} d\vec{r}, \tag{29}$$

$$\varepsilon_i^{\alpha} = \int \psi_i^{*\alpha}(\vec{r}) \left| -\frac{1}{2}\nabla^2 + V_N(\vec{r}) + \tilde{\phi}_I(\vec{r}) + \tilde{\mu}_I(\vec{r}) \right| \psi_i^{\alpha}(\vec{r}) d\vec{r}. \tag{30}$$

Using $\tilde{E}_{D\&C}$ as given in Eq. (18),

$$\begin{aligned}\frac{\partial\tilde{E}_{D\&C}}{\partial X_p} = & \sum_{\alpha}^{\Omega} \sum_{i}^{M^{\alpha}} \frac{\partial\eta_i^{\alpha}}{\partial X_p}\varepsilon_i^{\alpha} + \sum_{\alpha}^{\Omega} \sum_{i}^{M^{\alpha}} \eta_i^{\alpha} \\ & \times \left[\int \frac{\partial\psi_i^{*\alpha}}{\partial X_p} H\psi_i^{\alpha} d\vec{r} + \int \psi_i^{*\alpha} H \frac{\partial\psi_i^{\alpha}}{\partial X_p} d\vec{r} \right] \\ & + \sum_{\alpha}^{\Omega} \sum_{i}^{M^{\alpha}} \eta_i^{\alpha} \left[\int \psi_i^{*\alpha} \frac{\partial(V_N + \tilde{\phi}_I + \tilde{\mu}_I)}{\partial X_p} \psi_i^{\alpha} d\vec{r} \right] \\ & - \int \frac{\partial\tilde{\rho}_I}{\partial X_p} \left[\frac{1}{2}\tilde{\phi}_I + \tilde{\mu}_I \right] d\vec{r} - \int \tilde{\rho}_I \left[\frac{1}{2}\frac{\partial\tilde{\phi}_I}{\partial X_p} + \frac{\partial\tilde{\mu}_I}{\partial X_p} \right] d\vec{r} \\ & + \int \tilde{\mu}_I \frac{\partial\tilde{\rho}_I}{\partial X_p} d\vec{r} + \frac{\partial E_{NN}}{\partial X_p}. \end{aligned} \tag{31}$$

The second term in Eq. (31), involving basis derivatives, is the basis set correction, or Pulay[35] force, arising from the incompleteness in the basis set $\{\phi_k^{\alpha}\}$. More will be said about this term later. After combining terms and using the definition of $\tilde{\rho}_o$ given in Eq. (22), which is equivalently

$$\tilde{\rho}_o = \sum_{\alpha}^{\Omega} \sum_{i}^{M^{\alpha}} \eta_i^{\alpha} \psi_i^{*\alpha}(\vec{r}) \psi_i^{\alpha}(\vec{r}), \tag{32}$$

Eq. (31) can be written as

$$\begin{aligned}\frac{\partial\tilde{E}_{D\&C}}{\partial X_p} = & \sum_{\alpha}^{\Omega} \sum_{i}^{M^{\alpha}} \frac{\partial\eta_i^{\alpha}}{\partial X_p}\varepsilon_i^{\alpha} + \sum_{\alpha}^{\Omega} \sum_{i}^{M^{\alpha}} \eta_i^{\alpha} \\ & \times \left[\int \frac{\partial\psi_i^{*\alpha}}{\partial X_p} H\psi_i^{\alpha} d\vec{r} + \int \psi_i^{*\alpha} H \frac{\partial\psi_i^{\alpha}}{\partial X_p} d\vec{r} \right] \\ & + \int \tilde{\rho}_o \left[\frac{\partial V_N}{\partial X_p} + \frac{\partial\tilde{\phi}_I}{\partial X_p} + \frac{\partial\tilde{\mu}_I}{\partial X_p} \right] d\vec{r} - \int \tilde{\rho}_I \frac{\partial\tilde{\phi}_I}{\partial X_p} d\vec{r} \\ & - \int \tilde{\rho}_I \left[\frac{\partial\tilde{\mu}_I}{\partial X_p} \right] d\vec{r} + \frac{\partial E_{NN}}{\partial X_p}. \end{aligned} \tag{33}$$

Reordering and combining terms, the D&C gradient force simplifies to

$$\begin{aligned}\frac{\partial\tilde{E}_{D\&C}}{\partial X_p} = & \int \tilde{\rho}_o \left[\frac{\partial V_N}{\partial X_p} \right] d\vec{r} + \frac{\partial E_{NN}}{\partial X_p} + \sum_{\alpha}^{\Omega} \sum_{i}^{M^{\alpha}} \frac{\partial\eta_i^{\alpha}}{\partial X_p}\varepsilon_i^{\alpha} \\ & + \sum_{\alpha}^{\Omega} \sum_{i}^{M^{\alpha}} \eta_i^{\alpha} \left[\int \frac{\partial\psi_i^{*\alpha}}{\partial X_p} H\psi_i^{\alpha} d\vec{r} + \int \psi_i^{*\alpha} H \frac{\partial\psi_i^{\alpha}}{\partial X_p} d\vec{r} \right] \\ & + \int (\tilde{\rho}_o - \tilde{\rho}_I) \left[\frac{\partial\tilde{\phi}_I}{\partial X_p} + \frac{\partial\tilde{\mu}_I}{\partial X_p} \right] d\vec{r}. \end{aligned} \tag{34}$$

The first two terms in Eq. (34) are easily recognized as the traditional Hellmann–Feynman[36] force terms, although the

use of the output density $\tilde{\rho}_o$ instead of $\tilde{\rho}_I$ might be a little surprising. The third term is unique to D&C and we will call it the partition force, $F^P_{X_p}$. The fourth and fifth terms are the well known Pulay[35] and the density-fit correction[26,29] force terms, respectively. Clearly, the fifth term becomes zero if and when the input and output densities become equal. Similarly, the Pulay force will approach zero as the LCAO basis set $\{\phi^\alpha_k\}$ becomes more nearly complete.

Evaluation of the partition force,

$$F^P_{X_p} = \sum_\alpha^\Omega \sum_i^{M^\alpha} \frac{\partial \eta^\alpha_i}{\partial X_p} \varepsilon^\alpha_i \tag{35}$$

requires first finding the derivatives of the partitioned-occupation numbers,$\{\eta^\alpha_i\}$. In principle, these derivatives could be determined numerically by carrying out self-consistent calculations at two slightly different values of each coordinate for each atom and then approximating the derivatives as ratios of the finite changes $\Delta\eta^\alpha_i/\Delta X_p$. Such a computationally intensive procedure, however, is not very efficient since one could just as easily approximate the component forces in a similar way as $-\Delta\tilde{E}_{D\&C}/\Delta X_p$. Nevertheless, this procedure can and will be used in Sec. III B in order to demonstrate the validity of the formalism in an application to N_2. To the authors' knowledge a more efficient way of computing the set of derivatives, $\{\partial\eta^\alpha_i/\partial X_p\}$, and consequently evaluating the D&C gradient force [Eq. (34)] has not been given for the general case.

It should be pointed out that the sum of terms in Eq. (34), excluding the partition force, takes the form of the gradient force within the Harris energy (i.e., traditional "unpartitioned") model under certain conditions. This results by replacing the partitioned-occupation numbers $\{\eta^\alpha_i\}$ with the usual occupation numbers $\{n_i\}$ and restricting the partition sum to the single total system. With the usual filling of states, the occupation numbers $\{n_i\}$ under atom displacements can only change at the Fermi energy, and conservation of the number of electrons guarantees that the sum in Eq. (35) will always be zero or at least small. In contrast, this term will not in general be zero in the D&C method, as will be shown in Sec. III B.

III. APPLICATIONS

A. Methodology

In a recent paper[19] results for a number of molecular systems were given using the full SCPW method to assess both the self-consistent atom fragment (SCAF) and the non-self-consistent atom fragment (NSCAF) models, as used with simplified charge density models. The purpose of that work was to assess possible embedding approximations. The D&C results reported here use the same framework of numerical methods and approximations. In particular, basis functions in the present LCAO calculations are numerical atomic orbitals supplemented by diffuse s, p, and d Gaussian functions resulting in basis sets that are of approximate double-zeta quality. The LDA exchange-correlation approximation is that of Vosko, Wilk, and Nusair.[37] All integrations are carried out numerically using the three-dimensional Gaussian quadrature technique discussed in Ref. 20.

The energy in the NSCAF method without D&C (essentially the original form of the Harris energy[23]) reduces to a form with the input density formed from the superposition of spherically symmetrical atomic densities $\{\rho_k(\vec{r})\}$ in Eq. (16), omitting the sums over partial waves. This model[19] can be easily generalized to encompass the D&C approximation for the sum of one-electron energies [Eq. (5)]. The D&C-NSCAF method, like the original Harris energy (i.e., NSCAF), is non-self-consistent; however, it has been shown[3,4] to be a useful approximation for very large atomic clusters.

Forces on atoms in this work were evaluated in one of the two ways depending upon the energy models being used and the comparisons being made. In SCPW and NSCAF calculations, the forces can be determined using the well known analytical gradient formalism[26,29] with numerical integrations. However, as discussed in Sec. II D, evaluation of the analytical expression for the D&C gradient force is as yet numerically impractical and, thus, except for validation of the gradient force expression, D&C forces are found numerically by computing the total energy at two points on either side of the coordinate value of interest and evaluating $\Delta E/\Delta x$.

B. Divide and conquer force: N_2

Evaluation of the D&C gradient force [Eq. (34)] is complicated by the partition force term [Eq. (35)]. Although the partition force can be computed numerically, it is just as efficient to compute the total force directly as a numerical derivative of the D&C energy. However, for simple illustrative purposes, the gradient force and its components were calculated for the case of N_2 in the D&C(0) NSCAF model.

In Fig. 1(a), the N_2 binding energy is plotted as a function of bond distance for the D&C(0) NSCAF method as well as for several other related models.[38] No buffering is used in the D&C(0) approximation and therefore each of the two D&C(0) fragments consists of just a single N atom. The D&C(0)-SCPW and D&C(0)-NSCAF energy curves track one another rather closely, implying that except at small separations the contribution of self-consistency and higher $(l>0)$ partial waves to the D&C(0) model density is relatively small. This unusually good agreement of the D&C(0) energies is likely due to the large degree of spherical symmetry of the contributions of the N atoms in the D&C(0) models, since the non-D&C models, SCPW and NSCAF, produce considerably different curves. The close agreement of D&C(0) model energies is also reflected in their respective force curves [Fig. 1(b)] where the D&C(0)-SCPW and D&C(0)-NSCAF forces are close to one another except at small bond distances. The two D&C(0) force curves are also to a lesser extent close to the NSCAF force curve which again probably reflects the sphericity of their atomic contributions to their respective model electron densities.

A comparison of the D&C(0) NSCAF gradient force with the force calculated directly as the numerical derivative of the D&C(0) NSCAF energy is presented in Table I. The good

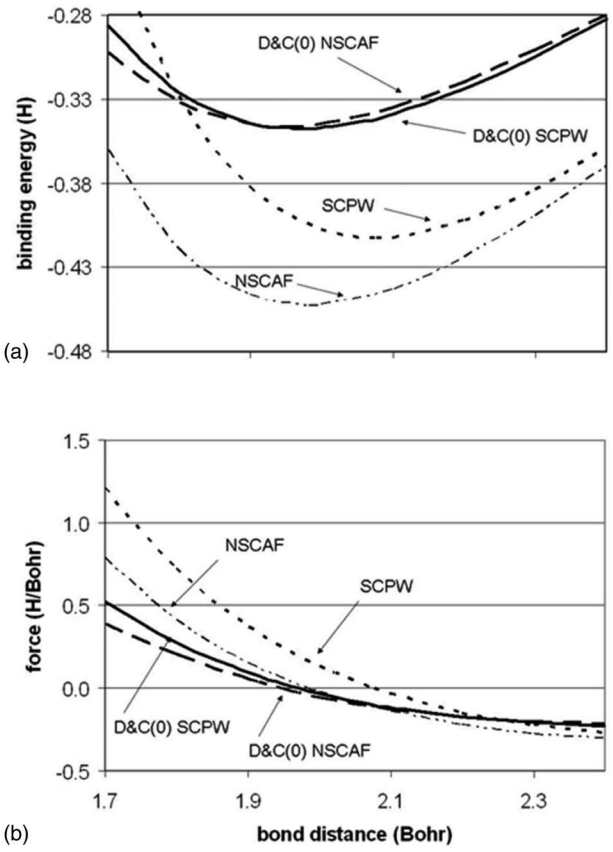

FIG. 1. N_2 (a) binding energy and (b) atom force curves for four different models discussed in the text. Bond distances are in a.u. (bohr) and binding energies are in hartrees. Forces are in units of hartrees/bohr.

agreement of these two independent evaluations of the force provides validation of the gradient force expression given in Eq. (34). The gradient force is further analyzed in terms of the contributions of the so called partition (P) force (Eq. (35)) and all other terms in Eq. (34), which we have chosen to call collectively the Harris (H) force. An interesting property of these two terms is that they are of about the same magnitude but are opposite in sign. Thus the gradient force has its zero at the bond distance (1.948 a.u.) where partition and Harris forces exactly cancel one another as Eq. (34) requires.

C. Divide and conquer example: Formamide molecule

The formamide molecule ($HCONH_2$, see Fig. 2) is a trivial case for D&C; nevertheless, its small size makes it simple to compare various levels of the D&C approximation (i.e., with or without buffering) with accurate KS results.[39] Computation of the differences within a single scheme has obvious advantages. Furthermore, the planar geometry of formamide simplifies illustration of various features of D&C revealed in density contour plots.

In Table II, structural equilibrium results for three levels of D&C approximation are given where in each case the molecule has been partitioned into two fragments, HCO and NH_2. For reference, standard KS[19] and experimental[42] results are also given. In all D&C calculations, zero-temperature Fermi statistics were used to determine the occupation numbers $\{n_i^\alpha\}$ defined by Eq. (11). For the partial-wave expansions in Eqs. (16) and (17), $l_{\max}=4$ was chosen for each atom.

The model labeled D&C(0) is the case of D&C with no buffer atoms for the two fragments and represents the lowest level of D&C approximation. Not surprisingly, D&C(0) produces large errors compared to the more accurate models, D&C(1) and D&C(2), discussed below. As expected, the C-N bond that connects the two fragments shows the largest error (i.e., 7% too short) due to the lack of any quantum interaction between the two atoms forming the bond. Some bond angles also exhibit large errors. For example, the angles C-N-H_c and O-C-H are too small by 18° and 19°, respectively.

Buffering each fragment with its nearest neighbor atom yields the D&C(1) results in Table II. In the case of the NH_2 fragment, the C atom and its basis set supplement the other atoms of the fragment (see Fig. 3). Similarly, the N atom and its basis set were added to those of the HCO fragment. As a result of this minimum amount of buffering [D&C(1)], the C

TABLE I. Binding energy (BE) (hartrees) of N_2 in the D&C(0) NSCAF model and a comparison of the corresponding gradient force (total force) and numerical energy derivative (dE/dx) as functions of the bond distance, R (bohr). Partition force (P force) and Harris force (H force) make up the total force (in hartrees/bohr) of Eq. (34).

R	BE	P force	H force	Total force	$-dE/dx$
1.70000	−0.30237	2.1794	−1.7884	0.3911	0.3904
1.80000	−0.33190	1.9944	−1.7879	0.2065	0.2066
1.90000	−0.34484	1.7618	−1.7040	0.0578	0.0580
1.94759	−0.34618	1.6461	−1.6461	0.0000	0.0001
2.00000	−0.34473	1.5212	−1.5749	−0.0537	−0.0536
2.10000	−0.33533	1.3037	−1.4326	−0.1289	−0.1288
2.20000	−0.31997	1.1248	−1.2991	−0.1743	−0.1741
2.30000	−0.30111	0.9860	−1.1856	−0.1996	−0.1996
2.40000	−0.28037	0.8806	−1.0945	−0.2139	−0.2139

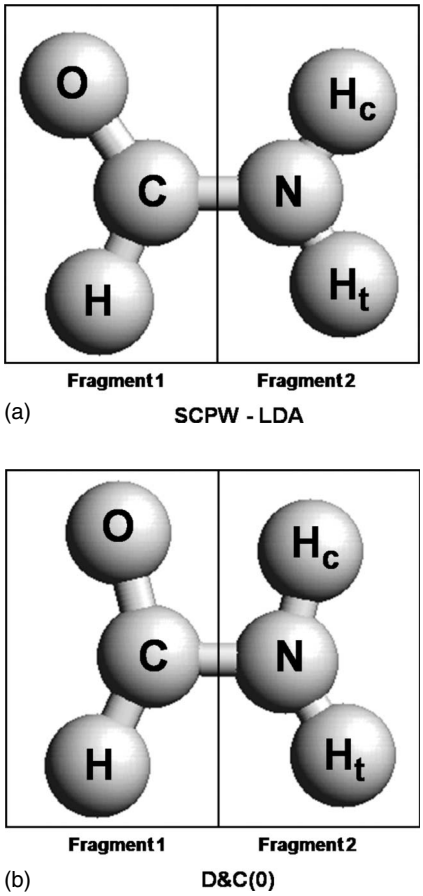

FIG. 2. (a) Equilibrium structure of the formamide molecule in the LDA. The cis and trans hydrogen atoms are labeled by subscripts c and t, respectively. (b) The equilibrium structure at the D&C(0) level (i.e., without any buffering), with partitioning into two fragments, NH_2 and COH. Buffering each fragment with just its nearest neighbor atom [i.e., D&C(1)] produces a structure which is indistinguishable from the SCPW-LDA structure shown in (a).

and N atoms are now fully coordinated within their respective fragments and the errors of D&C(0) are dramatically reduced (Table II). The C-N bond distance error of D&C(1) is less than 1% and errors in bond angle are less than 3°.

There are two ways to recapture standard KS results within the D&C framework. The simplest approach is to treat the entire cluster as a single D&C fragment. With no partitioning, effectively no D&C approximation is made. The second way is to buffer each of the Ω fragments with all the atoms outside each specific fragment. Of course this approach is the more inefficient, since one must solve the entire problem Ω times. Nevertheless, for a small molecule such as formamide, this second method can be easily carried out and provides a useful cross check of the computational procedures. The D&C(2) results in Table I were obtained in this way and indeed agree with the standard KS results[19] to within the numerical precision of the calculations.

The charge density of the formamide molecule and the effects of the partition functions are illustrated in Fig. 3. A partition function can be seen to have the effect of projecting a particular fragment's density from the total electron density. In the formamide case, the partitioning operator, for the NH_2 fragment, for example, effectively removes the density contribution of the fragment's buffer atoms [as seen in comparing Figs. 3(a) and 3(b)]. Similarly, it defines the NH_2 fragment as part of the whole system, as seen by comparing Figs. 3(b) and 3(e). This then minimizes the effect of truncation error on the fragment's contribution to the total density. The further out one buffers the contributing fragments, the more accurate the total density although convergence is not guaranteed to be uniform. When the partitioned densities [Figs. 3(b) and 3(d)] of the two fragments in the D&C(1) model are added together, the resulting density [Fig. 3(e)] is indistinguishable from the standard self-consistent KS density, at least to the level of resolution of the figure.

The ground state total energies (E) and kinetic energies (KEs) of formamide in the different models are tabulated in Table III. The virial theorem, which is exactly satisfied in density functional theory,[32] states that when the forces on the atoms are zero, the total and kinetic energies are equal in magnitude and opposite in sign. The fact that the calculated relation meets the ideal one rather well for the KS formamide results is indicative of the accuracy of the numerical integrations and the high quality of the basis sets. Not surprisingly, the virial theorem is less well satisfied by the D&C model where the kinetic energies tend to be too small. For reference, the approximate kinetic energies of the noninteracting

TABLE II. Equilibrium bond distances (in Å), bond angles (in deg), and binding energies (BEs) (in eV) for the formamide molecule ($HCONH_2$, see Fig. 2) using D&C with various levels of buffering. In each D&C model, the molecule was partitioned into the two fragments: HCO and NH_2. The D&C(0) notation denotes calculations without any buffering. D&C(1) indicates near neighbor buffering, whereas D&C(2) is complete buffering to all neighbors. Kohn–Sham (KS) results from Ref. 19 using SCPW and microwave experimental (Expt.) values from Ref. 40 are also given.

	Bond lengths					Bond angles				
Method	C-O	C-N	C-H	N-H_c	N-H_t	O-C-N	H-C-N	C-N-H_c	C-N-H_t	BE
D&C(0)	1.178	1.255	1.112	1.046	1.016	105.7	113.4	100.3	123.3	35.39
D&C(1)	1.211	1.361	1.120	1.022	1.013	124.9	113.2	116.7	118.6	28.88
D&C(2)	1.214	1.349	1.119	1.019	1.015	124.7	112.2	118.4	121.4	28.92
SCPW	1.214	1.350	1.119	1.019	1.016	124.9	111.9	119.0	121.3	28.92
Expt.	1.219	1.352	1.098	1.001	1.001	124.7	112.7	118.5	120.0	NA

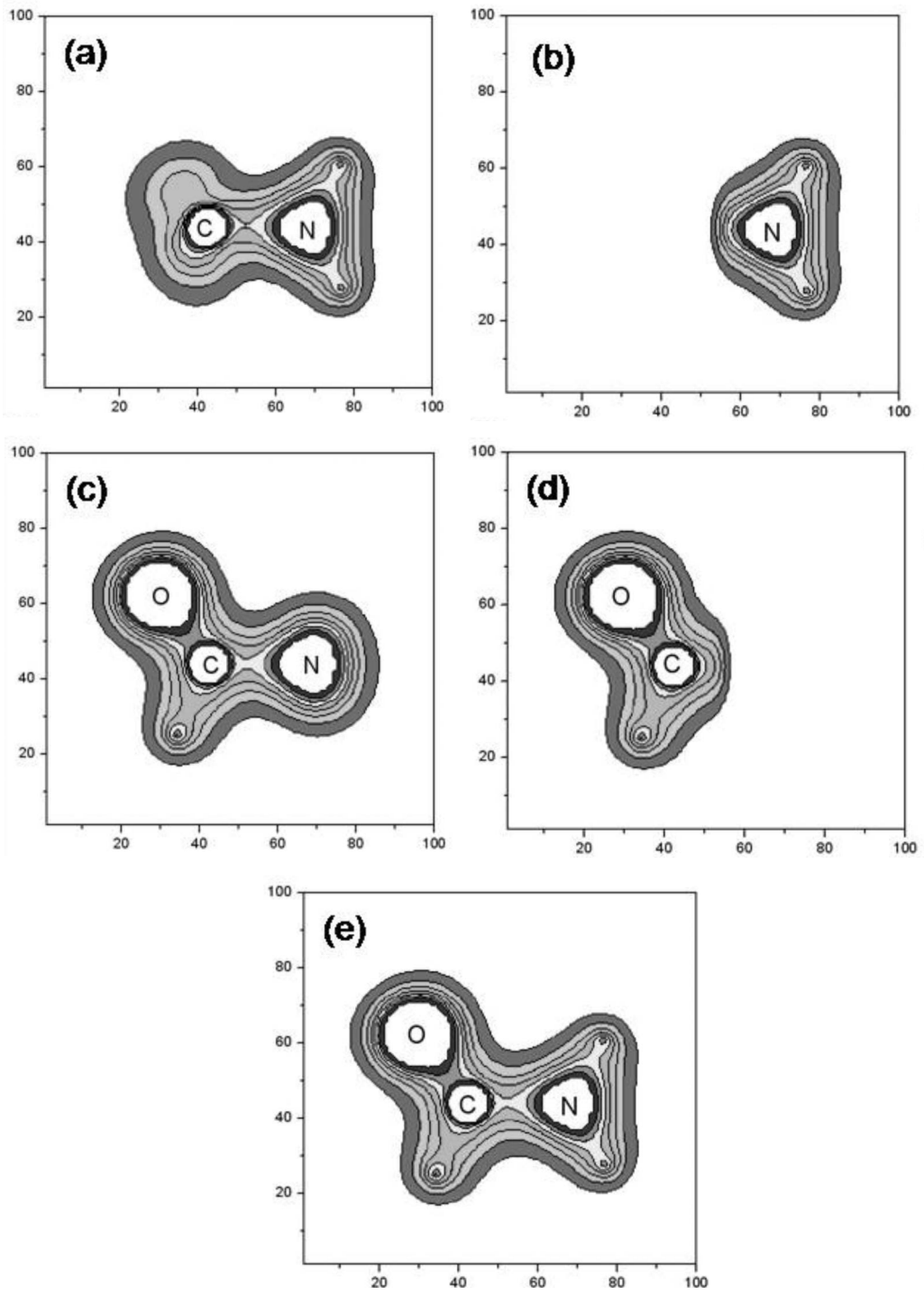

FIG. 3. Contour plots of the D&C fragments for formamide in the D&C(1) model discussed in the text. (a) Density of the fragment, NH_2, and its C buffer atom. (b) Density of the C-buffered NH_2 fragment, but here multiplied by its partition function [see Eq. (5)]. (c) Fragment, HCO, with its N buffer atom. (d) N-buffered HCO fragment density multiplied by its partition function. (e) Total density of formamide obtained by adding the partitioned densities in (b) and (d).

electron gas (K_0) are also given along with the differences (KE$-K_0$). It is interesting to note that this difference remains nearly constant across the different models, suggesting that the kinetic energy error originates mainly from errors in K_0 and the error is largely independent of the exchange-correlation terms of Eq. (26).

As further confirmation of the D&C gradient force expression [Eq. (34)], the components of forces on the atoms in the formamide molecule are tabulated in Table IV near the ground state for the D&C(1) NSCAF model. In agreement with the N_2 results (Sec. III B), the partition and Harris forces at equilibrium are equal in magnitude and opposite in

TABLE III. Ground state total energies (E), kinetic energies (KEs), and approximate kinetic energies of the noninteracting electron gas (K_0) for formamide using the different levels of D&C and the full KS model. Differences between KE and K_0 appear in the last column. All energies are in hartree at.u.

Model	E	KE	K_0	(KE−K_0)
D&C(0)	−168.8709	165.0586	164.0457	1.0129
D&C(1)	−168.6314	166.6905	165.6754	1.0151
D&C(2)	−168.6330	168.6401	167.6243	1.0158
KS	−168.6330	168.6333	167.6176	1.0157

sign. In addition, the components of the gradient force and the energy derivatives are close to zero. The sum of component forces is also nearly zero providing still more evidence of internal consistency

D. Example of divide and conquer self-consistent-partial-wave embedding: La bonding to β-Si_3N_4 crystal surface

It has been shown that D&C can describe structural features of a molecule to arbitrary accuracy (within the limits of the LDA) by including sufficient numbers of buffer atoms outside each of the partitions.[5] However, if the feature of interest is sufficiently localized within the molecule, convergence of D&C with respect to buffering may be optimized by choosing the fragments so that the boundaries of the partition in which the site is located are distant from the site. Nevertheless, it is proposed here that when D&C is being used as an embedding scheme, buffering is limited to just near neighbor atoms. Using the notation of previous sections, this limited form of D&C will be labeled D&C(1). In principle, if D&C(1) embedding results obtained with a particular partitioning scheme are shown to be sensitive to the degree of buffering, one can choose to either (1) increase the size of the central fragment containing the feature or (2) increase the level of buffering beyond D&C(1). Our results suggest that the first choice alone may often be satisfactory. In this section, we apply the embedding scheme to a study of the bonding of La atoms to a surface of the β-Si_3N_4 crystal, the prism plane that defines smooth grain boundary interfaces with matrix material in silicon nitride ceramics.

TABLE IV. For each atom in the planar formamide molecule, x and y components of the partition force (P force), the Harris force (H force), the total force, and the derivative of the D&C(1) NSCAF total energy (dE/dx). Atoms are near their equilibrium positions. Forces in units of hartrees/bohr.

Atom/axis	P force	H force	Total force	$-dE/dX$
N_x	0.1193	−0.1192	0.0002	−0.0006
N_y	0.0487	−0.0486	0.0001	0.0003
C_x	−0.2837	0.2840	0.0002	0.0006
C_y	−0.2974	0.2976	0.0002	0.0006
H_{t_x}	−0.0162	0.0157	−0.0005	−0.0006
H_{t_y}	0.2012	−0.2011	0.0001	0.0003
H_{c_x}	0.1712	−0.1712	0.0000	0.0009
H_{c_y}	−0.0526	0.0520	−0.0006	−0.0011
O_x	−0.0164	0.0164	0.0000	−0.0004
O_y	0.1334	−0.1332	0.0002	0.0000
H_x	0.0258	−0.0256	0.0002	0.0002
H_y	−0.0331	0.0330	−0.0002	0.0000

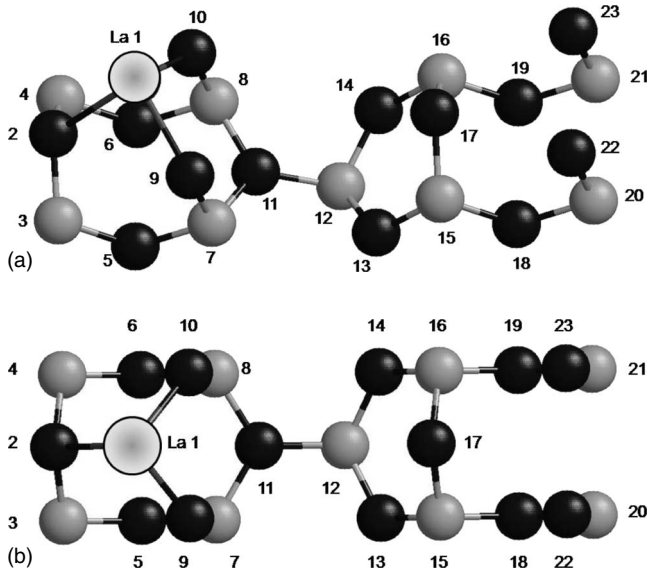

FIG. 4. Two perspective views of the $LaSi_9N_{13}$ atomic cluster model for the adsorption of La at the small hole site of the β-Si_3N_4 grain boundary prism plane. The dark atoms are N and the light atoms are Si; the La atom is the larger ball. The x axis is horizontal and runs from left to right with the origin at atom 2 and intersecting atom 17. Atoms 1, 2, 11, 12, and 17 lie in the xy plane. (a) is a view from approximately 60° above the xz plane. (b) is from above the xz plane and looking down the y axis.

Recent first-principles studies[41] of the segregation of rare-earth (RE) atoms to the prism plane of β-Si_3N_4 grain boundaries have used the 23-atom cluster model shown in Fig. 4. Calculations on this and other similar small cluster models led to the prediction that RE atoms would preferentially segregate to the "small hole" absorption site on the prism plane. These predictions were confirmed by high resolution transmission electron microscopy experimental data which showed that not only the relative numbers but also the bond distances of the RE atoms were in good agreement with the LDA atomic cluster calculations. The surprising success of these small cluster models naturally leads to an interest in determining the sensitivity of the results to model size. Not only can much larger clusters be treated, if useful, but there is also the usual question of size convergence. In addition, there is the new interest in using D&C(1) as an embedding method.

In order to address these issues, a series of model cluster calculations have been performed (see Table V) using the force on the La atom in each model to test the sensitivity of the equilibrium location of the La atom at the adsorption site. In all models described in Table V, the La atom is located at the equilibrium position computed for the largest non-D&C

TABLE V. Force components (La_x and La_y) on La atom located at the small hole absorption site of the β-Si_3N_4 grain boundary prism plane (see Fig. 4) for different atom cluster models. For all force evaluations, the La atom is located at the equilibrium position computed for it in the $LaSi_9N_{13}$ model with the full SCPW. All other atoms are fixed at experimentally determined[42] lattice positions. In the two D&C models, the two fragments are $LaSi_4N_6$ and Si_5N_7. The column "Atom roster" gives the range of atoms, as numbered in Fig. 4, included in each cluster model. Forces are in units of hartrees/bohr. Cluster binding energies (BEs) (in eV) are given in the last column. The last two rows give results for a model where basis sets on atoms of Si_5N_7 fragment are restricted to minimum (M) basis size.

Method	Model	Atom roster	La_x	La_y	BE
SCPW	$LaSi_4N_6$	1–11	−0.0030	−0.0027	−50.56
SCPW	$LaSi_5N_6$	1–12	0.0035	0.0036	−55.98
SCPW	$LaSi_5N_8$	1–14	−0.0026	−0.0068	−61.38
SCPW	$LaSi_7N_9$	1–17	−0.0021	0.0004	−80.36
SCPW	$LaSi_9N_{13}$	1–23	0.0000	0.0000	−101.97
D&C(1)	$LaSi_4N_6$-Si_5N_7	1–11 and 12–23	−0.0004	−0.0013	−106.32
SCPW min	$LaSi_4N_6$-$Si_5N_7(M)$	1–11 and 12–23	−0.0005	−0.0042	−85.25
D&C(1) min	$LaSi_4N_6$-$Si_5N_7(M)$	1–11 and 12–23	−0.0004	−0.0040	−88.31

model in the series; i.e., $LaSi_9N_{13}$. The locations of all other atoms in the clusters are fixed at their experimentally determined[42] β-Si_3N_4 crystalline solid lattice positions. In all calculations, the SCPW method was used with $l_{max}=2$. For the D&C calculations, the atom fragments $LaSi_4N_6$ and Si_5N_7 are buffered, respectively, by their near neighbor atoms 12 and 11 shown in Fig. 4. The last two rows of Table V give results where the basis sets on atoms within the Si_5N_7 fragment have been restricted to minimum (M) basis set size.

All models described in Table V contain atoms which are subsets of the atoms in the $LaSi_9N_{13}$ cluster, and they were chosen to systematically add atoms along the x direction. This series critically tests the sensitivity of the La forces to cluster size and should be even more demanding than adding atoms in all three directions where force cancellations can occur due to atoms located in opposite directions. However, it is clear that even the smallest cluster ($LaSi_4N_6$) does remarkably well compared to larger systems. To assess the impact of small forces on the equilibrium position, the La atom in $LaSi_4N_6$ was allowed to relax, resulting in changes in the x and y coordinates of only 0.020 and 0.002 Å. As expected, the model clusters approaching $LaSi_9N_{13}$ in size have nearly zero force components, although the convergence of the forces is not uniform, with the intermediate cluster $LaSi_5N_8$ having the largest La force component (0.0068 hartrees/bohr). In general, the accuracy of the forces obtained in the D&C approximations are quite adequate for most purposes.

The results indicate that the equilibrium location of the La atom at the adsorption site of the first fragment is relatively insensitive to the atoms in the second (Si_5N_7) fragment. Nor does increasing the cluster size from $LaSi_7N_9$ to $LaSi_9N_{13}$ significantly affect the results. Using minimum basis sets for atoms in the Si_5N_7 fragment increases the La_y force component from near zero to only about −0.004 hartrees/bohr, and this result is independent of the D&C(1) approximation.

IV. CONCLUSION

In a sequel to a previous paper[19] in which the authors used the SCPW framework to study the convergence of molecular bond distances and the Harris total energy with respect to approximate representations of the input electronic charge density, the present paper investigated the use of D&C as an embedding method to extend the SCPW method to larger atomic clusters. It has been shown that D&C can be easily used as an efficient embedding technique when modeling, for example, impurities in solids.

The discussion of D&C included derivation of the LDA electronic kinetic energy as well as a new gradient force expression that accurately determines the derivative of the D&C total energy regardless of the level of buffering employed. In general systems, however, the computational effort required for its evaluation will restrict its usefulness. Even so, the new force expression may prove useful in special circumstances when forces calculated directly from the total energy or by still other means need confirmation or verification. The adaptation of SCPW to include D&C was illustrated, and the new kinetic energy and gradient force expressions were validated by applications of D&C to simple cases of N_2 and formamide ($COHNH_2$).

A study of adsorption of La atoms at the β-Si_3N_4 grain boundary prism plane demonstrated that D&C incorporated into the SCPW framework forms an efficient embedded cluster technique, based on the sensitivity of results to fragment size and to representation of the host electronic density. Results suggest that atomic clusters of only modest size, and simple levels of embedding such as D&C(1)-SCPW are capable of determining relevant structural properties of localized impurities. The rapid convergence of adsorption site structural data for small and simple models of the host environment further confirms the concept of the nearsightedness of electronic matter[2] and the accuracy of atomic cluster models in systems with localized bonding.

ACKNOWLEDGMENTS

Research sponsored by the Division of Materials Sciences and Engineering, U.S. Department of Energy under contract with UT-Battelle, LLC. The authors appreciate discussions with D. E. Ellis and J. R. Morris and thank P. F. Tortorelli and C. L. Fu for reviewing the manuscript.

---

*Deceased.

[1] W. Yang, Phys. Rev. Lett. **66**, 1438 (1991); Phys. Rev. A **44**, 7823 (1991).

[2] W. Kohn, Phys. Rev. Lett. **76**, 3168 (1996).

[3] D. York, J. P. Lu, and W. Yang, Phys. Rev. B **49**, 8526 (1994).

[4] J. P. Lu and W. Yang, Phys. Rev. B **49**, 11421 (1994).

[5] Q. Zhao and W. Yang, J. Chem. Phys. **102**, 9598 (1995).

[6] W. Yang and T.-S. Lee, J. Chem. Phys. **103**, 5674 (1995).

[7] T. Zhu, W. Pan, and W. Yang, Phys. Rev. B **53**, 12713 (1996).

[8] T. Zhu, W. Pan, and W. Yang, Theor. Chem. Acc. **96**, 2 (1997).

[9] S. L. Dixon and K. M. Merz, J. Chem. Phys. **107**, 879 (1997).

[10] T.-S. Lee, J. P. Lewis, and W. Yang, Comput. Mater. Sci. **12**, 259 (1998).

[11] O. Warschkow, J. M. Dyke, and D. E. Ellis, J. Comput. Phys. **143**, 70 (1998).

[12] A. van der Vaart, D. Suarez, and K. M. Merz, J. Chem. Phys. **113**, 10512 (2000).

[13] J. M. Cabrera-Trujillo and J. Robles, Phys. Rev. B **64**, 165408 (2001).

[14] D. E. Ellis and O. Warschkow, Coord. Chem. Rev. **238-239**, 31 (2003).

[15] F. Shimojo, R. K. Kalia, A. Nakano, and P. Vashishta, Comput. Phys. Commun. **167**, 151 (2005).

[16] A. Nakano, R. K. Kalia, K. Nomura, A. Sharma, P. Vashishta, F. Shimojo, A. C. T. van Duin, W. A. Goddard, R. Biswas, and D. Srivastava, Comput. Mater. Sci. **38**, 642 (2007).

[17] M. Sironi, A. Genoni, M. Civera, S. Peiraccini, and M. Ghitti, Theor. Chem. Acc. **117**, 685 (2007).

[18] S. Y. Wu and C. S. Jayanthi, Phys. Rep. **358**, 1 (2002).

[19] F. W. Averill and G. S. Painter, Phys. Rev. B **73**, 235125 (2006).

[20] F. W. Averill and G. S. Painter, Phys. Rev. B **50**, 7262 (1994).

[21] S. Goedecker, Rev. Mod. Phys. **71**, 1085 (1999).

[22] K. Morokuma, Philos. Trans. R. Soc. London, Ser. A **360**, 1149 (2002).

[23] J. Harris, Phys. Rev. B **31**, 1770 (1985).

[24] W. M. C. Foulkes and R. Haydock, Phys. Rev. B **39**, 12520 (1989).

[25] M. Born and J. R. Oppenheimer, Ann. Phys. **84**, 457 (1927).

[26] F. W. Averill and G. S. Painter, Phys. Rev. B **41**, 10344 (1990).

[27] L. J. Sham, Phys. Rev. B **32**, 3876 (1985), and references therein.

[28] F. W. Averill and G. S. Painter, Phys. Rev. B **46**, 2498 (1992).

[29] B. Delley, J. Chem. Phys. **92**, 508 (1990); **94**, 7245 (1991).

[30] G. S. Painter, Phys. Rev. B **23**, 1624 (1981).

[31] A. R. Williams, J. Kubler, and C. D. Gelatt, Jr., Phys. Rev. B **19**, 6094 (1979).

[32] F. W. Averill and G. S. Painter, Phys. Rev. B **24**, 6795 (1981).

[33] J. P. Perdew, K. Burke, and M. Ernzerhof, Phys. Rev. Lett. **77**, 3865 (1996); **78**, 1396 (1997).

[34] P. Legrand and F. Perrot, J. Phys.: Condens. Matter **13**, 287 (2001).

[35] P. Pulay, Mol. Phys. **17**, 197 (1969).

[36] R. P. Feynman, Phys. Rev. **56**, 340 (1939).

[37] S. H. Vosko, L. Wilk, and M. Nusair, Can. J. Phys. **58**, 1200 (1980).

[38] Yang in Ref. 1 also computed the binding energy curve for N_2 using a model very similar to D&C(0)-SCPW, however, with $X\alpha$ exchange-correlation and Slater-type basis sets.

[39] In the new version of the SCPW technique, the D&C model is the standard and KS results are recaptured by treating the entire cluster as a single D&C fragment.

[40] E. Hirota, R. Sugisaki, C. J. Nielsen, and G. O. Sorensen, J. Mol. Spectrosc. **49**, 251 (1974).

[41] P. F. Becher, G. S. Painter, N. Shibata, R. L. Satet, M. J. Hoffmann, and S. J. Pennycook, Mater. Sci. Eng., A **422**, 85 (2006).

[42] P. Yang, H.-K. Fun, I. A. Rahman, and M. I. Saleh, Ceram. Int. **21**, 137 (1995).